

# Modified graphite and graphene electrodes for high-performance lithium ion hybrid capacitors

Ji Hoon Lee · Weon Ho Shin · Soo Yeon Lim ·  
Byung Gon Kim · Jang Wook Choi

Received: 23 September 2013 / Accepted: 13 January 2014 / Published online: 31 January 2014  
© The Author(s) 2014. This article is published with open access at Springerlink.com

**Abstract** Lithium ion capacitors (LICs) have recently received considerable attention as a new class of energy storage system because they possess the combined advantages of lithium ion batteries and supercapacitors. LICs typically consist of activated carbon cathodes and pre-lithiated graphite anodes. Despite the promising electrochemical performance, most LICs still hold room for further improvement in terms of power density, which is largely related to the limited (de)intercalation kinetics of graphite. In an attempt to address these limited kinetics, we have developed a simple treatment to modify the morphology and surface characteristics of graphite engaging hydrogen peroxide. The treatment increases the exposed edge planes and generates more stable solid-electrolyte-interphase layers, which facilitate substantially improved power and cycling performance of the graphite anodes. Especially when integrated with a urea-reduced graphene cathode, the modified graphite-based LIC exhibits significantly higher energy and power densities compared to those of the pristine graphite-based and other reported counterparts.

**Keywords** Lithium ion capacitor · Graphene · Graphite · Enolization · Hybrid capacitor

**Electronic supplementary material** The online version of this article (doi:10.1007/s40243-014-0022-9) contains supplementary material, which is available to authorized users.

J. H. Lee · W. H. Shin · S. Y. Lim · B. G. Kim ·  
J. W. Choi (✉)

Graduate School of EEWS (Energy, Environment, Water, and Sustainability) and Center for Nature-inspired Technology (CNiT), KAIST Institute NanoCentury, Korea Advanced Institute of Science and Technology (KAIST), 291 Daehakro, Yuseong-gu, Daejeon 305-701, Republic of Korea  
e-mail: jangwookchoi@kaist.ac.kr

## Introduction

Energy storage systems (ESSs) are expected to play an important role in resolving various energy and environmental issues because ESSs are essential means for efficient electricity distribution as well as use of renewable energy resources [1–8]. Along this direction, supercapacitors have fulfilled critical functions such as ‘energy smoothing’ and ‘momentary energy loading’ in grid-scale ESSs by utilizing their high rate capabilities and long cycle lives [7–14]. However, most supercapacitors still suffer from limited energy densities originating from the intrinsic charge/discharge mechanism based on adsorption/desorption of carrier ions, thus restricting the range of applications. As an effort to overcome this limitation, a new class of ESSs, so-called lithium ion capacitors (LICs), has been recently developed and has shown promising electrochemical performance [15–30]. As the name indicates, LIC is a combined system between Li ion batteries (LIBs) and supercapacitors. In this hybrid system, the cathode works based on the adsorption/desorption of ions as in supercapacitors, whereas the anode operates as a Li ion source by engaging the insertion/desertion processes of Li ions as in LIBs. Typical LICs exhibit energy densities around 30 Wh/kg, which is more than three times larger than those of electrical double layer capacitors [16, 26].

Although a variety of carbonaceous materials have been considered for LIC anodes [23, 28, 31–37], pre-lithiated graphite has been the most widely used one, which is usually due to its unique voltage characteristic that charge and discharge take place at a low constant voltage at 0.1 V (vs. Li/Li<sup>+</sup>) over nearly the entire capacity. This voltage character enables high operating voltage (~4 V) and stable solid-electrolyte-interphase (SEI) formation throughout cycling, as thoroughly discussed in previous literature [15].

This low constant voltage renders graphite clearly more desirable for high energy density and long cycle life as compared to other carbonaceous materials including hard carbon (HC), graphene, and carbon nanotubes.

Despite these well-established advantages, the graphite anode suffers from relatively sluggish kinetics for (de)insertion of Li ions during charge and discharge, restricting the rate capability of the entire cell. In particular, it has been known that the lithiation process (charge) is most rate-limiting [18, 19, 28, 38] among a series of continuous electrochemical events. The graphite could be replaced by other carbonaceous materials such as HC that can afford to facilitate rapid kinetics for Li (de)insertion. However, the improved rate performance, in turn, deteriorates the specific capacity and thus the cell energy density, indicating a trade-off between different carbonaceous materials [23, 28, 30]. For the same purpose of increasing the rate performance, ball-milling processes were also employed for graphite during the electrode fabrication but leading to only limited success [18].

Herein, we develop a simple hydrogen peroxide treatment for graphite LIC anodes, which remarkably improves the rate capabilities of the cells without sacrificing other advantageous properties of graphite, such as high specific capacity and long cycle life. The enhanced rate performance was associated with more desirable particle morphology and SEI formation for efficient Li ion diffusion in the graphite anode. Moreover, in an attempt to increase the cell energy density further, the most commonly used activated carbon cathode was replaced by a functionalized graphene cathode, thus addressing both power and energy density issues simultaneously.

## Experimental section

### Preparation of modified graphite

The graphite anode was modified to improve rate performance. Hereafter, we denote the modified graphite as MG. For preparation of MG, 1 g of pristine graphite (PG, Alfa Aesar. Synthetic, APC 7-11, micron, 99 %) was first introduced in 100 mL of 5 wt% hydrogen peroxide ( $\text{H}_2\text{O}_2$ , Sigma Aldrich) aqueous solution, and the solution was then heated to 70 °C for 1 h. Next, the suspension was sonicated at a power of 200 W for 1 h. Once the sonication was completed, MG was filtrated through alumina membrane filters (pore size 0.2  $\mu\text{m}$ , Whatman) and was then washed with deionized (DI) water and ethanol several times.

### Preparation of urea-reduced graphene oxide (URGO)

The functionalized graphene was used as a LIC cathode to increase the energy density. For this purpose, reduced

graphene oxide (GO) was prepared following the procedure reported previously [15]. Briefly, GO suspension was first prepared from graphite (Alfa Aesar) by a modified Hummer's method and was then reduced by a urea treatment. 1 g of graphite and 0.5 g of sodium nitrate ( $\text{NaNO}_3$ , Sigma Aldrich) were introduced into 23 mL of sulfuric acid ( $\text{H}_2\text{SO}_4$ , Sigma Aldrich) and stirred vigorously at 0 °C for 3 h. Then, 3.5 g of potassium permanganate ( $\text{KMnO}_4$ , Sigma Aldrich) was gradually added at 30 °C until the color of the suspension turned dark gray. 46 mL of DI water was added very slowly until the temperature reached 98 °C. Lastly, warm DI water (60 °C, 140 mL) and  $\text{H}_2\text{O}_2$  (35 wt%, 5 mL, Sigma Aldrich) were added, and the suspension was maintained at 60 °C for 3 h. The final bright brown solution was filtered and washed with DI water several times. 200 mg of GO powder was added to 200 mL of DI water. Finally, the GO solution was reduced using urea ( $\text{H}_2\text{N}-\text{CO}-\text{NH}_2$ , Sigma Aldrich). 6 g of urea was added to 200 mL of the GO solution with a concentration of 1 mg/mL, and the mixed solution was refluxed at 98 °C for 35 h. After the reduction process, the color of the solution was black. The urea-reduced GO (URGO) solution was then filtered and washed with DI water and ethanol several times to remove any residual impurities.

### Characterization of the graphite anode

The surface functional groups of both MG and PG were characterized by X-ray photoelectron spectroscopy (XPS, Thermo VG scientific, Sigma Probe). A high-resolution dispersive Raman microscope (Raman, Horiba Jobin-Yvon) was used to characterize the degree of defects in the graphitic array. The chemical compositions of both types of graphite were investigated by element analysis (EA, Flash 2000 series). Finally, field emission-scanning electron microscope (FE-SEM, Sitrion) was used to observe the morphologies of both types of graphite.

### Electrochemical test

In full-cell configurations, both types of graphite were used as anode materials, whereas AC (Kurary, YP-80F) and URGO were used as cathode materials. The anodes were prepared by first preparing slurries. The active materials, super-P (Timcal), and poly (vinylidene difluoride) (PVDF, Sigma Aldrich) were dispersed in 1-methyl-2-pyrrolidone (NMP, Sigma Aldrich) in a weight ratio of 8:1:1. The slurries were then cast onto copper foil. The AC cathode was prepared through the same procedure except that AC and aluminum foil were used as the active material and current collector, respectively. After the casting, all of the electrodes were dried in a vacuum oven at 70 °C for 12 h. From control experiments that dictate available capacities

for further charging to 4 V after the pre-lithiation, the mass ratio of both electrodes was determined to be cathode : anode = 2:1. The actual mass loadings of the active materials were 2 and 1 mg/cm<sup>2</sup> for the cathode and anode, respectively. A mixture of ethylene carbonate and diethylene carbonate (1:1 = v:v) containing 1 M lithium hexafluorophosphate (LiPF<sub>6</sub>) and 3 wt% vinylene carbonate (PANAX E-TEC, Korea) was used as electrolyte. Polypropylene membranes (Celgard 2400) were used as separators. The cell assembly was performed in an argon-filled glove box.

Prior to full-cell characterization, the graphite anodes underwent pre-lithiation by employing a half-cell configuration in which lithium metal (Hoshen) was used as both the counter and reference electrodes. The same electrolyte and separators were used as in the full-cells. For the pre-lithiation, the cells went through two full galvanostatic cycles in the voltage range of 0.005–1.5 V (vs. Li/Li<sup>+</sup>) followed by a charging process down to 0.05 V (vs. Li/Li<sup>+</sup>) at a 0.1 C (=0.037 A/g) rate. After the pre-lithiation, LIC full-cells were fabricated by assembling the cathodes and the pre-lithiated graphite anodes in 2,032 coin cells. Electrochemical performance of LIC full-cells was evaluated by using a WBCS 3000 battery cycler (Wonatech, Korea) at 25 °C. For the charge, the constant current constant voltage (CCCV) mode was applied by holding the cell voltage at 4 V for 10 min before the discharge. For the discharge, the constant current mode was employed. Specific capacity (mAh/g), energy density (Wh/kg), and power density (W/kg) were calculated based on the combined weight of the active materials from both sides of the electrodes. As in the previous reports [15], the energy density was calculated by obtaining the integrated area of the galvanostatic discharge curve (voltage vs. capacity). The power density was calculated by dividing the obtained energy density by discharge time.

## Results and discussion

The SEM images taken before and after the hydrogen peroxide treatment are presented in Fig. 1. While both PG and MG show similar morphologies in low magnification images (Fig. 1a, c), they show clearly distinctive morphologies in a higher magnification (Fig. 1b, d). PG shows relatively smooth surfaces over most particles (Fig. 1b), whereas MG shows sharp edges (Fig. 1d and Fig. S1 in Electronic Supplementary Material) as in other similar cases that underwent mild oxidation treatments [39, 40]. It is anticipated that the exposure of the sharp edges is associated with the hydrogen peroxide treatment that rearranges the inter-particle structures while etching the edge carbon atoms. The oxidation takes place mainly at the

edges because a majority of dangling bonds to be oxidized are located at the edges [41, 42]. The edge-oriented etching of carbon atoms in MG was also supported by Raman spectroscopy results (Fig. S2 in Electronic Supplementary Material). The intensity ratio between D band (~1,350 cm<sup>-1</sup>) and G band (~1,580 cm<sup>-1</sup>) generally reflects the degree of defects in the graphitic array. As compared with PG, MG exhibits a more intensified D band, suggesting that a larger number of defects were generated in MG, which is indeed commensurate with carbon etching at the edges during the hydrogen peroxide treatment.

The effect of the hydrogen peroxide was first examined in lithium half-cell measurements. As displayed in Fig. 2a, both types of graphite show similar CV curves in the entire potential range of 0.005–2.5 V (vs. Li/Li<sup>+</sup>) when measured at 0.03 mV/s. The lithiation and delithiation take place at ~0.01 and 0.2 V (vs. Li/Li<sup>+</sup>), respectively, which are consistent with previous reports [19]. The reductive peaks at ~0.8 V (vs. Li/Li<sup>+</sup>) corresponding to SEI formation were also observed for both types of graphite. However, unlike PG, MG exhibits a small broad peak around 1.7 V (vs. Li/Li<sup>+</sup>) (inset of Fig. 2a), which is ascribed to functional groups at the edges of graphite that enable an enolization process with Li ions. This phenomenon seemingly results from the fact that the surface functional groups generated during the hydrogen peroxide treatment are sequentially oxidized to carbonyl containing groups such as carbonate, carboxyl, carbonyl, and lactone groups [41–43], and these groups react with Li ions based on  $>C=O + Li^+ + e^- \leftrightarrow >C-O-Li$ . Similar enolization processes have been reported in other previous reports [15, 44–46].

The enolized functional groups on the surfaces of graphite have a significant effect on the cycle lives of graphite anodes. For the testing of cycle life, both cells were tested at C/10 (=0.037 A/g) for the first five cycles to generate stable SEI layers and then at C/3.3 (=0.111 A/g) for subsequent cycles. As displayed in Fig. 2b, while both samples show similar initial specific capacities, the MG anode exhibits much better cycling performance compared to that of the PG anode. After 30 cycles, the MG anode retains 102 % of the original capacity, whereas the PG anode retains only 54 % of the original capacity. The improved cycle life of the MG anode results from formation of stable SEI layers [41, 42, 47–50] because it has been known that lithium carboxylic salts (enolized functional groups in the current study) can be chemically bonded to the outer SEI layers generated from electrolyte reduction which has turned out to be more stable during repeated cycles than those formed directly on the graphite surfaces. In detail, the chemically bonded SEI layers have been previously found to (1) adhere robustly to the edge planes owing to the role of the enolized surface functional groups

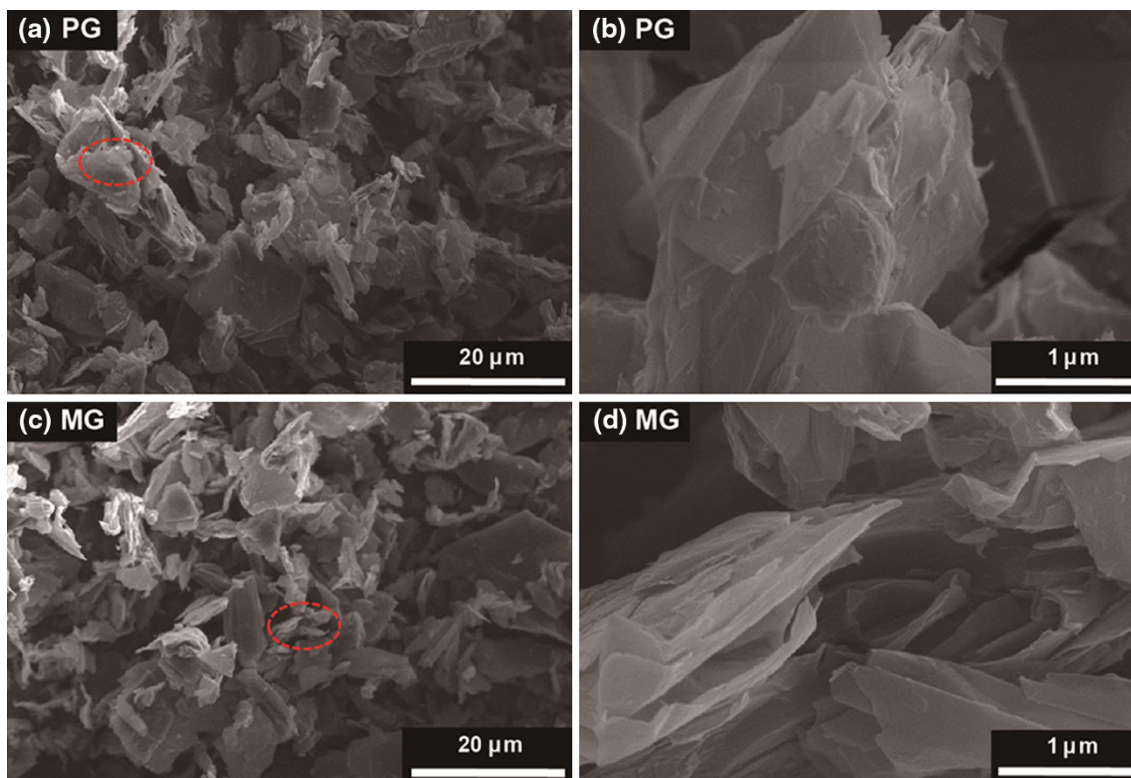


**Fig. 1** a, b Low and high magnification SEM images of PG. c, d SEM images of MG with the same magnifications as in (a) and (b)

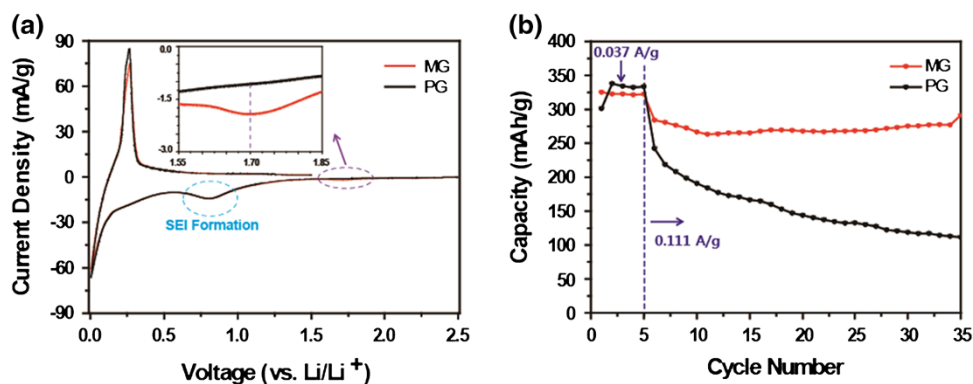


**Fig. 2** a CV data for MG and PG as anodes in lithium half-cell configurations. (Inset) magnified data in the voltage range of 1.55–1.85 V (vs.  $\text{Li/Li}^+$ ) indicative of lithium enolization. b Cycling performance of MG and PG anodes in lithium half-cell

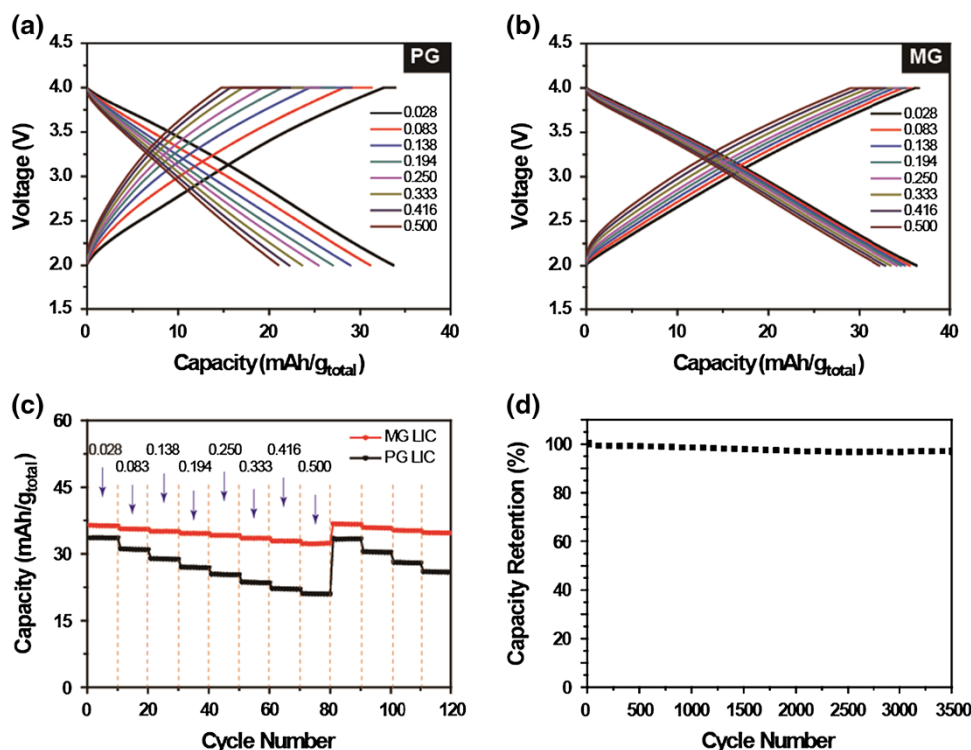
servicing as glue or bonding agents for  $\text{Li}_2\text{CO}_3$  based SEI layers [41], (2) block the co-intercalation of bulky counter ions such as  $\text{PF}_6^-$  [51], and (3) thus prevent the exfoliation of exposed edge planes. It is also anticipated that the well-developed edge planes of the MG play a role in persistent Li (de)intercalation and therefore the better cycle life. Although XPS analyses were performed from the expectation of distinctive chemical characteristic of MG, O1s spectra appear quite similar for both cases, which is likely due to the limited number of the functional groups formed

configurations. The current density is 0.037 A/g for the first five cycles and 0.111 A/g for the subsequent cycles. The mass loadings of both active electrodes are 1 mg/cm<sup>2</sup>

at the edges of MG. This observation is also consistent with the small reductive CV peak in Fig. 2a corresponding to the enolization. Thus, the amount of chemically bonded SEI layers is predicted to be limited. However, the modified SEI layers can still play a critical role for efficient Li diffusion because Li (de)intercalation takes place mainly through the edge planes where the modified SEI layers are in direct contact.

EA and XPS were performed to clarify the relationship between the surface functional groups and element

**Fig. 3** The galvanostatic charge/discharge profiles of **a** PG and **b** MG LICs measured at various current densities from 0.028 to 0.5 A/g<sub>total</sub>. For each cycle, the CC and CCCV modes were applied for the discharge and charge, respectively. **c** Rate capabilities of both LICs at various current densities in the range of 0.028–0.5 A/g<sub>total</sub>. The shown capacities are discharge capacities. **d** Cycle life of MG LIC measured at a current density of 0.138 A/g<sub>total</sub> (=4 C). All of the data in this figure are based on the weights of both active electrodes (AC cathode: 2 mg/cm<sup>2</sup>, MG/PG anode: 1 mg/cm<sup>2</sup>)



contents. (Table 1 in Electronic Supplementary Material) In the bulk EA analysis, as expected, carbon signal shows up dominantly for both types of graphite. In the XPS analysis, however, the detected surface oxygen amount was different (6.94:4.48 wt% = MG:PG), supporting that the carbonyl containing functional groups were generated during the hydrogen peroxide treatment (Fig. S3 in Electronic Supplementary Material).

After pre-lithiation processes for the graphite anodes, the full-cells consisting of the graphite anodes and the AC cathodes were evaluated under galvanostatic testing. From Fig. 3a and b, the following points are noticeable in LIC operations: (1) The MG LIC shows far better rate performance. As the current density increases, the specific capacity of the PG LIC drops more rapidly compared to that of the MG LIC. This distinctive trend is summarized in Fig. 3c. While the MG LIC shows a slightly higher capacity at the lowest rate of 0.028 A/g<sub>total</sub>, the capacity difference between both LICs becomes more significant with increased current rate. When the current density increases by 18 times from 0.028 to 0.5 A/g<sub>total</sub>, the MG LIC retains 88.9 % of the original capacity (36 → 32 mAh/g<sub>total</sub>). However, for the same increase in the current density, the PG LIC retains only 62.3 % (33.6 → 21 mAh/g<sub>total</sub>). (2) In both cases of LICs, it was seen that the charging processes are more kinetically limiting than the discharging processes, as the charging capacities are smaller at all of the current rates, and this gap becomes more apparent at increased current rates. This observation

reflects that lithiation processes of graphite are more kinetically sluggish than delithiation processes. Remarkably, after the hydrogen peroxide treatment, the charging kinetics becomes markedly improved, diminishing the capacity differences between charging and discharging processes, which suggests that the exposed edge planes and modified SEI layers make Li ion diffusion into graphite more efficient [38, 41, 42, 49]. This trend is also consistent with the half-cell results in Figs. 2b and S4 (Electronic Supplementary Material). (3) The increased capacity of the MG LIC at the lowest current rate is likely to be associated with modified staging processes after the hydrogen peroxide treatment. As displayed in Fig. 4, while both types of graphite anodes exhibit almost same capacities, the MG anode shows a longer discharge stage I at ~0.1 V (vs. Li/Li<sup>+</sup>) and a shorter discharge stage II at ~0.14 V (vs. Li/Li<sup>+</sup>) as compared to those of the PG anode [52]. It is anticipated that the extended stage I at lower potential contributes to the cell capacity increase at the lowest current rate. In detail, when the LIC is under discharge condition, the potential of the AC cathode swings down while that of graphite anode gradually increases until their potential gap touches the lower cut-off voltage of 2 V [15]. Therefore, the longer discharge stage I at the lower anode potential enables the cathode potential to move more down so that the total LIC capacity can be increased.

Furthermore, the MG LIC exhibits stable cycling over a large number of cycles. As shown in Fig. 3d, when measured at 4C (=0.138 A/g<sub>total</sub>), the MG LIC loses only 3 %

of its original capacity after 3,500 cycles, indicating that the modified SEI layers are stable over repeated cycles and therefore the LIC cells satisfy the one of the most important conditions in LIC operation. The cycling performance of the PG LIC is also compared in Fig. S5 (Electronic Supplementary Material). When measured at 2C ( $=0.083 \text{ A/g}_{\text{total}}$ ), the PG LIC shows continuous capacity fading in the first 50 cycles ( $33 \rightarrow 28 \text{ mAh/g}_{\text{total}}$ ), but thereafter its capacity becomes saturated at  $30 \text{ mAh/g}_{\text{total}}$ , which might be related to an SEI stabilization process.

In an effort to further improve the overall cell capacity at each current rate, we also integrated functionalized graphene cathode in replacement of the AC cathode. In a previous study [15], we have demonstrated that the LIC cathode consisting of URGO delivers substantially higher capacities compared to those of the electrodes based on AC or hydrazine-reduced graphene oxide. Thus, in the current investigation, we combined the URGO cathode with the MG anode, and its rate capability is comparatively presented in Fig. 5a. The URGO-MG cell shows increased capacities at both high and low current rates. For example, the URGO-MG cell exhibits 23 and 11 % higher capacities

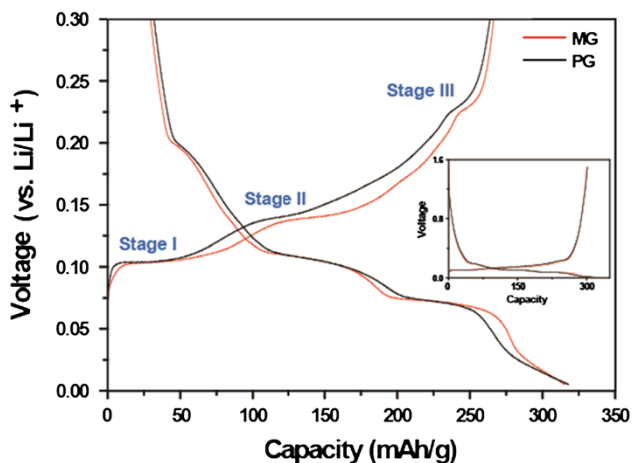
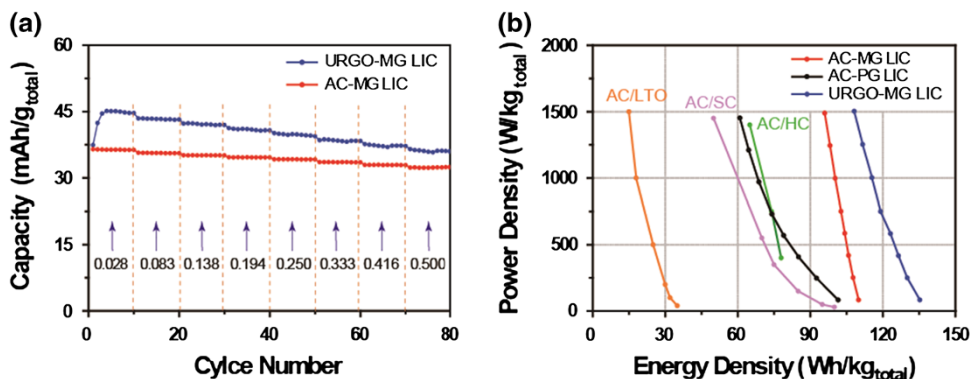


**Fig. 4** The galvanostatic charge/discharge curves of MG and PG measured at a current density of  $0.037 \text{ A/g}$  in the voltage range of  $0.005\text{--}1.5 \text{ V}$  (vs.  $\text{Li/Li}^+$ ). The inset shows the charge/discharge curves in the entire potential range

**Fig. 5 a** Rate capabilities of URGO-MG and AC-MG LICs at various current densities from  $0.028$  to  $0.5 \text{ A/g}_{\text{total}}$ . **b** A Ragone plot (energy density vs. power density) for the LICs in this study alongside others reported recently. All of the data in this figure are based on the weights of both active electrodes (Cathode:  $2 \text{ mg/cm}^2$ , Anode:  $1 \text{ mg/cm}^2$ )



at  $0.62$  and  $13.8 \text{ C}$ , respectively, compared to the AC-MG cell, implying that the new electrodes on both the anode and cathode sides improve both energy and power densities of overall LICs simultaneously.

Based on these electrochemical results, we have constituted a Ragone plot (Fig. 5b) that also includes the data from other representative LIC cells in previous reports, such as AC-HC [28], AC-soft carbon (SC) [23], and AC-lithium titanate ( $\text{Li}_4\text{Ti}_5\text{O}_{12}$ ; LTO) [27], for comparison. From this plot, the following points can be addressed: (1) As described in Fig. 3a–c, the AC-MG cell shows higher energy densities at given power densities compared to those of the AC-PG cell. For instance, while the AC-PG LIC shows an energy density of  $61 \text{ Wh/kg}_{\text{total}}$  at a power density of  $1,452 \text{ W/kg}_{\text{total}}$ , the AC-MG LIC delivers a 1.55 times higher energy density of  $95 \text{ Wh/kg}_{\text{total}}$  at a similar power density of  $1,489 \text{ W/kg}_{\text{total}}$ . (2) The URGO-MG LIC shows even higher power and energy densities. The URGO-MG LIC provides  $12.7\text{--}25.3$  and  $33.2\text{--}77.5$  % increased energy densities than those of AC-MG and AC-PG LICs, respectively, in the power density range covered in this study. Apparently, the energy density of the URGO-MG LIC is superior to those of other reported LICs (1.4–7.2 times) in the given power density range: AC/LTO ( $15\text{--}35 \text{ Wh/kg}_{\text{total}}$ ) [26], AC/SC ( $50\text{--}100 \text{ Wh/kg}_{\text{total}}$ ) [22], and AC/HC ( $65\text{--}78 \text{ Wh/kg}_{\text{total}}$ ) [27]. (3) The energy density of the URGO-MG LIC reaches  $135 \text{ Wh/kg}_{\text{total}}$ . Although other cell components than electrodes should be counted for fair comparison with other established systems, the energy density of  $135 \text{ Wh/kg}_{\text{total}}$  based on the electrode mass only must be still at least close to those of the conventional secondary batteries such as lead-acid battery ( $30\text{--}40 \text{ Wh/kg}_{\text{total}}$ ), nickel-cadmium battery ( $50\text{--}60 \text{ Wh/kg}_{\text{total}}$ ), and nickel-metal hydride battery ( $60\text{--}100 \text{ Wh/kg}_{\text{total}}$ ) [5, 12].

## Conclusion

In conclusion, in an attempt to address the limited rate performance of conventional LICs, the graphite anode, the very

limiting cell component for rate performance, was modified by a simple hydrogen peroxide treatment. After the treatment, the MG anode is endowed with chemically bonded SEI layers and exposed edge planes both of which facilitate more efficient Li diffusion, especially during charging (lithiation) processes. In both Li half-cell and LIC full-cell tests, the enhanced Li diffusion is reflected by the improved rate capability and stable capacity retention over a large number of cycles. Moreover, when paired up with the established functionalized graphene cathode, the so-called URGO, the LIC cell exhibits excellent energy and power densities, which are also superior to those of previously reported analogous systems. In particular, the energy density of the URGO-MG LIC approaches those of the existing battery systems. Overall, these new anode and cathode materials, respectively, address the causes of the limited power and energy densities in previous LICs. The current investigation delivers a lesson that even well-known electrode materials can still be modified further to improve key electrochemical properties of energy storage cells.

**Acknowledgments** This work was financially supported by the National Research Foundation of Korea (NRF) grant funded by the Korea government (MEST) (NRF-2012-M1A2A2026587).

**Open Access** This article is distributed under the terms of the Creative Commons Attribution License which permits any use, distribution, and reproduction in any medium, provided the original author(s) and the source are credited.

## References

- Yang, Z.G., Zhang, J.L., Kintner-Meyer, M.C.W., Lu, X.C., Choi, D.W., Lemmon, J.P., Liu, J.: Electrochemical energy storage for green grid. *Chem. Rev.* **111**, 3577–3613 (2011)
- Etacheri, V., Marom, R., Elazari, R., Salitra, G., Aurbach, D.: Challenges in the development of advanced Li-ion batteries: a review. *Energy Environ. Sci.* **4**, 3243–3262 (2011)
- Hall, P.J., Mirzaei, M., Fletcher, S.I., Sillars, F.B., Rennie, A.J.R., Shitta-Bey, G.O., Wilson, G., Cruden, A., Carter, R.: Energy storage in electrochemical capacitors: designing functional materials to improve performance. *Energy Environ. Sci.* **3**, 1238–1251 (2010)
- Armand, M., Tarascon, J.M.: Building better batteries. *Nature* **451**, 652–657 (2008)
- Tarascon, J.M., Armand, M.: Issues and challenges facing rechargeable lithium batteries. *Nature* **414**, 359–367 (2001)
- Ibrahim, H., Ilinca, A., Perron, J.: Energy storage systems: characteristics and comparisons. *Renew. Sustain. Energy Rev.* **12**, 1221–1250 (2008)
- Choi, B.G., Yang, M., Hong, W.H., Choi, J.W., Huh, Y.S.: 3D macroporous graphene frameworks for supercapacitors with high energy and power densities. *ACS Nano* **6**, 4020–4028 (2012)
- Jeong, H.M., Lee, J.W., Shin, W.H., Choi, Y.J., Shin, H.J., Kang, J.K., Choi, J.W.: Nitrogen-doped graphene for high-performance ultracapacitors and the importance of nitrogen-doped sites at basal planes. *Nano Lett.* **11**, 2472–2477 (2011)
- Zhang, J.T., Zhao, X.S.: On the configuration of supercapacitors for maximizing electrochemical performance. *ChemSusChem* **5**, 818–841 (2012)
- Sharma, P., Bhatti, T.S.: A review on electrochemical double-layer capacitors. *Energy Convers. Manag.* **51**, 2901–2912 (2010)
- Stoller, M.D., Park, S.J., Zhu, Y.W., An, J.H., Ruoff, R.S.: Graphene-based ultracapacitors. *Nano Lett.* **8**, 3498–3502 (2008)
- Simon, P., Gogotsi, Y.: Materials for electrochemical capacitors. *Nat. Mater.* **7**, 845–854 (2008)
- Burke, A.: Ultracapacitors: why, how, and where is the technology. *J. Power Sources* **91**, 37–50 (2000)
- Lee, J.H., Park, N., Kim, B.G., Jung, D.S., Im, K., Hur, J., Choi, J.W.: Restacking-inhibited 3D reduced graphene oxide for high performance supercapacitor electrodes. *ACS Nano* (2013). doi:10.1021/nm4040734
- Lee, J.H., Shin, W.H., Ryou, M.-H., Jin, J.K., Kim, J.-H., Choi, J.W.: Functionalized graphene for high performance lithium ion capacitors. *ChemSusChem* **5**, 2328–2333 (2012)
- Park, M.S., Lim, Y.G., Kim, J.H., Kim, Y.J., Cho, J., Kim, J.S.: A novel lithium-doping approach for an advanced lithium ion capacitor. *Adv. Energy Mater.* **1**, 1002–1006 (2011)
- Cericola, D., Kotz, R.: Hybridization of rechargeable batteries and electrochemical capacitors: principles and limits. *Electrochim. Acta* **72**, 1–17 (2012)
- Sivakkumar, S.R., Milev, A.S., Pandolfo, A.G.: Effect of ball-milling on the rate and cycle-life performance of graphite as negative electrodes in lithium-ion capacitors. *Electrochim. Acta* **56**, 9700–9706 (2011)
- Sivakkumar, S.R., Nerkar, J.Y., Pandolfo, A.G.: Rate capability of graphite materials as negative electrodes in lithium-ion capacitors. *Electrochim. Acta* **55**, 3330–3335 (2010)
- Sivakkumar, S.R., Pandolfo, A.G.: Evaluation of lithium-ion capacitors assembled with pre-lithiated graphite anode and activated carbon cathode. *Electrochim. Acta* **65**, 280–287 (2012)
- Naoi, K.: ‘Nanohybrid capacitor’: the next generation electrochemical capacitors. *Fuel Cells* **10**, 825–833 (2010)
- Amatucci, G.G., Badway, F., Du Pasquier, A., Zheng, T.: An asymmetric hybrid nonaqueous energy storage cell. *J. Electrochem. Soc.* **148**, A930–A939 (2001)
- Schroeder, M., Winter, M., Passerini, S., Balducci, A.: On the use of soft carbon and propylene carbonate-based electrolytes in lithium-ion capacitors. *J. Electrochem. Soc.* **159**, A1240–A1245 (2012)
- Aravindan, V., Chuilin, W., Madhavi, S.: High power lithium-ion hybrid electrochemical capacitors using spinel LiCrTiO<sub>4</sub> as insertion electrode. *J. Mater. Chem.* **22**, 16026–16031 (2012)
- Cericola, D., Novak, P., Wokaun, A., Kotz, R.: Hybridization of electrochemical capacitors and rechargeable batteries: an experimental analysis of the different possible approaches utilizing activated carbon, Li<sub>4</sub>Ti<sub>5</sub>O<sub>12</sub> and LiMn<sub>2</sub>O<sub>4</sub>. *J. Power Sources* **196**, 10305–10313 (2011)
- Du Pasquier, A., Plitz, I., Menocal, S., Amatucci, G.: A comparative study of Li-ion battery, supercapacitor and nonaqueous asymmetric hybrid devices for automotive applications. *J. Power Sources* **115**, 171–178 (2003)
- Jung, H.G., Venugopal, N., Scrosati, B., Sun, Y.K.: A high energy and power density hybrid supercapacitor based on an advanced carbon-coated Li<sub>4</sub>Ti<sub>5</sub>O<sub>12</sub> electrode. *J. Power Sources* **221**, 266–271 (2013)
- Kim, J.H., Kim, J.S., Lim, Y.G., Lee, J.G., Kim, Y.J.: Effect of carbon types on the electrochemical properties of negative electrodes for Li-ion capacitors. *J. Power Sources* **196**, 10490–10495 (2011)
- Konno, H., Kasashima, T., Azumi, K.: Application of Si–C–O glass-like compounds as negative electrode materials for lithium hybrid capacitors. *J. Power Sources* **191**, 623–627 (2009)

30. Shin, W.H., Jeong, H.M., Kim, B.G., Kang, J.K., Choi, J.W.: Nitrogen-doped multiwall carbon nanotubes for lithium storage with extremely high capacity. *Nano Lett.* **12**, 2283–2288 (2012)
31. Wu, Z.S., Ren, W.C., Wen, L., Gao, L.B., Zhao, J.P., Chen, Z.P., Zhou, G.M., Li, F., Cheng, H.M.: Graphene anchored with Co<sub>3</sub>O<sub>4</sub> nanoparticles as anode of lithium ion batteries with enhanced reversible capacity and cyclic performance. *ACS Nano* **4**, 3187–3194 (2010)
32. Wu, Z.S., Ren, W.C., Xu, L., Li, F., Cheng, H.M.: Doped graphene sheets as anode materials with superhigh rate and large capacity for lithium ion batteries. *ACS Nano* **5**, 5463–5471 (2011)
33. Endo, M., Kim, C., Nishimura, K., Fujino, T., Miyashita, K.: Recent development of carbon materials for Li ion batteries. *Carbon* **38**, 183–197 (2000)
34. Wang, G.X., Shen, X.P., Yao, J., Park, J.: Graphene nanosheets for enhanced lithium storage in lithium ion batteries. *Carbon* **47**, 2049–2053 (2009)
35. Wang, Q., Li, H., Chen, L.Q., Huang, X.J.: Monodispersed hard carbon spherules with uniform nanopores. *Carbon* **39**, 2211–2214 (2001)
36. Liu, X.M., Huang, Z.D., Oh, S.W., Zhang, B., Ma, P.C., Yuen, M.M.F., Kim, J.K.: Carbon nanotube (CNT)-based composites as electrode material for rechargeable Li-ion batteries: a review. *Compos. Sci. Technol.* **72**, 121–144 (2011)
37. Buiel, E., Dahn, J.R.: Li-insertion in hard carbon anode materials for Li-ion batteries. *Electrochim. Acta* **45**, 121–130 (1999)
38. Zaghbi, K., Song, X., Guerfi, A., Kostecki, R., Kinoshita, K.: Effect of particle morphology on lithium intercalation rates in natural graphite. *J. Power Sources* **124**, 505–512 (2003)
39. Buqa, H., Golob, P., Winter, M., Besenhard, J.O.: Modified carbons for improved anodes in lithium ion cells. *J. Power Sources* **97–8**, 122–125 (2001)
40. Zhao, H.P., Ren, J.G., He, X.M., Li, J.J., Jiang, C.Y., Wan, C.R.: Purification and carbon-film-coating of natural graphite as anode materials for Li-ion batteries. *Electrochim. Acta* **52**, 6006–6011 (2007)
41. Ein-El, Y., Koch, V.R.: Chemical oxidation: a route to enhanced capacity in Li-ion graphite anodes. *J. Electrochem. Soc.* **144**, 2968–2973 (1997)
42. Peled, E., Menachem, C., Bar-Tow, D., Melman, A.: Improved graphite anode for lithium-ion batteries: chemically bonded solid electrolyte interface and nanochannel formation. *J. Electrochem. Soc.* **143**, L4–L7 (1996)
43. Nakajima, T., Gupta, V., Ohzawa, Y., Koh, M., Singh, R.N., Tressaud, A., Durand, E.: Electrochemical behavior of plasma-fluorinated graphite for lithium ion batteries. *J. Power Sources* **104**, 108–114 (2002)
44. Chen, H., Armand, M., Demailly, G., Dolhem, F., Poizot, P., Tarascon, J.M.: From biomass to a renewable LiC<sub>6</sub>O<sub>6</sub> organic electrode for sustainable Li-ion batteries. *ChemSusChem* **1**, 348–355 (2008)
45. Xu, W., Read, A., Koech, P.K., Hu, D.H., Wang, C.M., Xiao, J., Padmaperuma, A.B., Graff, G.L., Liu, J., Zhang, J.G.: Factors affecting the battery performance of anthraquinone-based organic cathode materials. *J. Mater. Chem.* **22**, 4032–4039 (2012)
46. Song, Z.P., Xu, T., Gordin, M.L., Jiang, Y.B., Bae, I.T., Xiao, Q.F., Zhan, H., Liu, J., Wang, D.H.: Polymer-graphene nanocomposites as ultrafast-charge and discharge cathodes for rechargeable lithium batteries. *Nano Lett.* **12**, 2205–2211 (2012)
47. Kumar, T.P., Stephan, A.M., Thayananth, P., Subramanian, V., Gopukumar, S., Renganathan, N.G., Raghavan, M., Muniyandi, N.: Thermally oxidized graphites as anodes for lithium-ion cells. *J. Power Sources* **97–8**, 118–121 (2001)
48. Menachem, C., Peled, E., Burstein, L., Rosenberg, Y.: Characterization of modified NG7 graphite as an improved anode for lithium-ion batteries. *J. Power Sources* **68**, 277–282 (1997)
49. Menachem, C., Golodnitsky, D., Peled, E.: Effect of mild oxidation of natural graphite (NG7) on anode-electrolyte thermal reactions. *J. Solid State Electr.* **5**, 81–87 (2001)
50. Menachem, C., Wang, Y., Flowers, J., Peled, E., Greenbaum, S.G.: Characterization of lithiated natural graphite before and after mild oxidation. *J. Power Sources* **76**, 180–185 (1998)
51. Besenhard, J.O., Winter, M., Yang, J., Biberacher, W.: Filming mechanism of lithium-carbon anodes in organic and inorganic electrolytes. *J. Power Sources* **54**, 228–231 (1995)
52. Winter, M., Besenhard, J.O., Spahr, M.E., Novak, P.: Insertion electrode materials for rechargeable lithium batteries. *Adv. Mater.* **10**, 725–763 (1998)